OPEN ACCESS

Journal of Science & Cycling
Breakthroughs in Cycling & Triathlon Sciences

Original Article

Wear analysis of bicycle chain joints

Martin Rank-Isepp [1,*], **Oliver Koch** [1], **Simon Graf** [1] and **Manuel Oehler** [2]

Received: 18 September 2025 **Accepted:** 8 January 2026 **Published:** 5 February 2026

[1] Chair of Machine Elements, Gears and Tribology (MEGT), RPTU University Kaiserslautern-Landau (RPTU), Gottlieb-Daimler-Str. 42, 67663 Kaiserslautern, Germany

[2] Chair of Drive Technology, Ruhr University Bochum, Universitätsstraße 150, 44801 Bochum, Germany

Correspondence

Martin Rank-Isepp

Chair of Machine Elements, Gears and Tribology (MEGT), RPTU University Kaiserslautern-Landau (RPTU), Gottlieb-Daimler-Str. 42, 67663 Kaiserslautern, Germany

martin.rank-isepp@rptu.de

Abstract

The rapid electrification of bicycles has fundamentally transformed drivetrain dynamics, leading to significantly higher loads on mechanical components such as chains. Unlike in traditional bicycles, where wear and efficiency losses primarily concerned competitive riders, the widespread adoption of e-bikes and other high-performance bicycles has made these issues critical for everyday cycling. Increased torque and sustained power assistance place unprecedented mechanical and tribological demands on drivetrains, making durability, friction reduction, and efficiency vital considerations for both manufacturers and users. As a result, research and testing methods that were once used mainly for industrial chain applications are increasingly relevant for the cycling industry. This study addresses these emerging challenges by adapting proven methodologies from mechanical and automotive engineering. Through controlled laboratory testing, bicycle chains and lubricants can be evaluated under standardized conditions that replicate real-world usage scenarios. Such testing does not only enable precise comparisons between different chain and lubricant systems but also provides insight into the fundamental wear mechanisms and efficiency losses occurring under varying loads, speeds, and environmental conditions. The approach supports the tailored design of drivetrain components for diverse cycling applications, including urban e-bikes, high-speed track bicycles, and rugged mountain bikes. By bridging disciplines, this work paves the way for innovations that enhance performance, reliability, and sustainability in modern cycling. A model procedure is presented here based on three exemplary high-speed track-bike scenarios. The focus is on the implementation of the experimental strategy and the derivation of the methodology.

Keywords

Chain drive; wear; bicycle drive; tribology; sustainability; track bike; e-bike

1 Introduction

The global push towards sustainable mobility has triggered a renaissance in bicycle-based transport, particularly electric bicycles (e-bikes), which are becoming increasingly relevant as mass transportation solutions (Galatoulas, Genikomsakis, & Ioakimidis, 2020). The rise of bike-sharing platforms and growing urban infrastructure for bicycles indicate a shift in societal and political priorities. However, with this increased utilization, technological aspects of bicycle systems are gaining importance as well (Fishman & Cherry, 2016). Investments in e-bike technologies are still difficult to quantify precisely (Nosratzadeh, et al., 2025), but the entrance of original equipment manufacturer (OEM) into the e-bike sector signals its growing financial attractiveness. At the same time, suppliers from the automotive industry are beginning to respond to this market with new developments and innovations (Contò & Bianchi, 2023).

This growing interest puts the focus on components with high relevance for maintenance and efficiency, specifically, the drivetrain system. Long-lasting and low-maintenance systems are increasingly demanded by operators, especially in the context of fleet usage, which has prompted the optimization of maintenance strategies and downtime planning (Grau-Escolano, Bassolas, & Vicens, 2024). Central to these goals is the minimization of friction and wear, which are critical for extending maintenance intervals and increasing overall energy efficiency. In particular, the tribological systems within the bicycle are of significant relevance (Liew, Matthews, Dao, & Li, 2025). The chain drive plays a decisive role in this context, and prior studies have explored improvements in geometry e.g., spur gear adaptations (Baglioni, Cianetti, & Landi, 2012), materials (Li, Sosa, Andersson, & Olofsson, 2016), and lubrication strategies (Kozlov, Egorov, & Belogusev, 2017) also under adverse environmental conditions such as rain (Shen, Rahim, & Rahman, 2022). While some efforts have focused directly on the chain itself, many studies rely on system-level tests (Smit, van der Zwaard, Janssen, & Janssen, 2023) or simplified tribometer experiments (Aubert, Roizard, Grappe, & Lallemand, 2023). However, these methods face inherent limitations. Tribometers offer only approximate boundary conditions, while full drivetrain test benches are typically time-intensive and limited to system-level energy balances. Also, one of the most crucial tribological contacts is the chain joint, the sliding contact of pin and the bushing of the inner link. As the chain joint continuously circulates within the chain drive during operation, direct investigation of the contact interface is not readily feasible. Therefore, different testing methods are necessary.

Bicycle chains differ in their design from industrial roller chains. Both types consist of inner and outer links. The outer links are formed by pins press-fitted into the outer plates. The inner links of industrial roller chains comprise bushings press-fitted into the inner plates, with a freely rotating roller mounted on each bushing. In contrast, a bicycle chain often features an integrated bush design in which the bush is formed directly by the inner link plates. Instead of a separate cylindrical bush, the inner plates include symmetrically shaped, longitudinally split collars that function as the bearing surface for the rollers (Figure 1) (Patentnr. U.S. Patent No. 5,226,857 A, 1993).

Therefore, established testing methods must be adapted to this specific design.

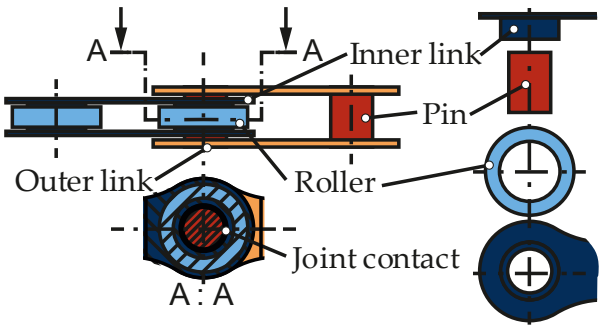

Figure 1. Structural design of bicycle chains

The necessity of more precise analysis methods becomes even more evident in light of recent simulation-based approaches. As demonstrated by ZHANG (Zhang & Tak, 2021) , the validation of computational loss models in e-bike drives revealed that a better understanding of individual loss mechanisms is required for accurate system-level simulations. This mirrors similar challenges found in industrial chain applications, where detailed understanding of tribological contact is essential.

To close the gap between simplified laboratory setups and complex system tests, the Chain Joint Tribometer (CJT) was developed and refined (Meffert, Oehler, & Sauer, 2021). In this test rig, individual chain joints are subjected to defined tensile loads and swivel angles. The loading can be dynamically controlled, allowing both realistic loads and freely defined model cycles to be applied. The CJT enables precise, targeted measurements of friction (Rank, Meffert, Oehler, & Koch, 2022) and real-time wear (Becker & Sauer, 2019) in the chain joint under controlled and realistic loading conditions. Using the CJT, effective prototype evaluations for optimizing both joint wear (Rank, et al., 2023) and frictional losses (Bobzin, et al., 2023) have been demonstrated. In addition, simulations based on multibody system models (MBS) and elasto-hydro-dynamic lubrication (EHL) models can be used to derive joint-level loading data for CJT validation (Simo Kamga, Meffert, Magyar, Oehler, & Sauer, 2022).

A key advantage of the CJT methodology is its capacity for load simplification. By focusing on dynamic loads and excluding static load scenarios, i.e. constant force at stationary deflection, the testing time can be significantly reduced without sacrificing validity. In combination with established wear analysis techniques (Sappok & Sauer, 2015), extensive wear investigations of the bicycle chains are possible. Current research demonstrates that the CJT can reproduce realistic loads and that the measured data show a high degree of agreement with system-level tests (Becker, Meffert, & Sauer, 2019). However, experimentally measured input data are essential for these tests. Such data is already widely available from competitive cycling (Gardner, Martin, Martin, Barras, & Jenkins, 2007) and can be effectively used for both laboratory and field calibration. The availability of high-resolution measurement devices (Menke, Shaw, & Zhang, 2024) and validated methodologies for evaluating data quality (Worn & Dwyer, 2019) further supports this approach.

Using MBS models (Omar, 2014), joint-specific load spectra can be derived from real-world use cases (Becker A. , 2020). This feature is becoming increasingly relevant as power densities in general e-bike usage approach those of competitive cycling, especially in disciplines like BMX sprinting, where instantaneous power outputs can exceed $P = 2\,\mathrm{kW}$ (Debraux, Manolova, Soudain-Pineau, & Hourde, 2013). For modern e-bikes, performance levels of $P = 250\,\mathrm{W}$ are observed (Arango, Lopez, & Ceren, 2021). Speed pedelecs can even reach system power levels of up to $P = 4\,\mathrm{kW}$ (Van den Steen, de Geus, Cappelle, & Vanhaverbeke, 2022). Consequently the performance requirements of chains are becoming more critical, even in everyday use. With common chain pitch dimensions of $p = 1/2\,"$, the load levels correspond to those

seen in industrial roller chains ((NAM), 2006). However, wider links are used for industrial roller chains. Therefore, joint pressures σ are lower and the joints are structurally stronger than bicycle chains ((NATG), 2018). Also, industrial roller chains differ in their bushing design, typically using single-piece bushings. It is reasonable to assume that the split bushings of bicycle chains may adversely affect wear behavior and lubrication dynamics.

This study demonstrates that established industrial test methodologies can be adapted to optimize the tribosystem of bicycle chain joints. The CJT test rig is further developed and used for exemplary wear tests. In parallel, the process chain from system-level load collection, through MBS simulation, to the derivation of chain joint-specific input parameters for CJT experiments is presented. A surface analysis, which is state of the art in industrial applications and enables the evaluation of worn contacts, is also presented.

2 Material and Methods

2.1 Chain Joint Tribometer

The CJT enables isolated loading of individual chain joints. The test rig consists essentially of two main modules (Figure 2). In the tensile force module, a linear actuator is used to simulate the chain tension force F_t by fixing the inner link of the chain. The angular motion module, which represents the kinematic articulation of the joint, holds the outer link. For testing, both defined static and dynamic tensile forces can be applied.

The stationary configuration of the chain joint allows for the acquisition of measurement data that would otherwise be inaccessible due to the spatial motion of the chain in circulating drivetrain systems. For instance, the elongation of the joint can be captured in real time via displacement sensors (Figure 3). Displacement is measured by using eddy-current sensors *Waycom Type T2-G-KA-VK23*, featuring a resolution of 0.25 µm and a linearity of 2 %. Calibration is carried out using a reference probe with an accuracy of 1 µm.

In addition, by measuring torque before and after the joint, the actual joint friction can be determined, independent of other machine elements such as bearings or seals that would otherwise influence the measurement. The torque measurement is performed using an *HBM Type TB02* transducer, force measurements by an *HBM Type U9C* load cell. Both sensors have an accuracy class of 0.2.

To operate the CJT, two key input variables are required: the chain tension force F_t and the angular position α, both defined as time-discrete signals. These can be freely specified. To provide realistic input data, multibody simulation (MBS) models are typically employed. Such models enable the representation of even complex drivetrain layouts with minimal effort. Furthermore, due to the flexible design of the CJT, tests can be performed on various chain geometries and sizes.

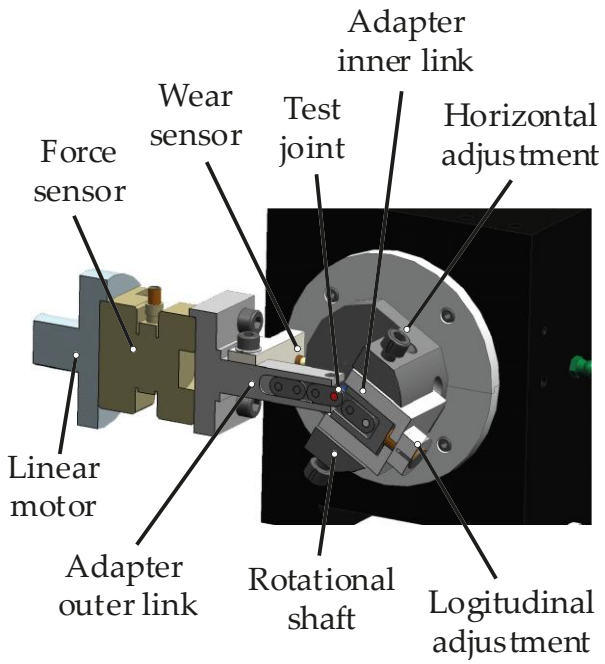

Figure 2. Cross section of CJT testing module with mounted bicycle chain link

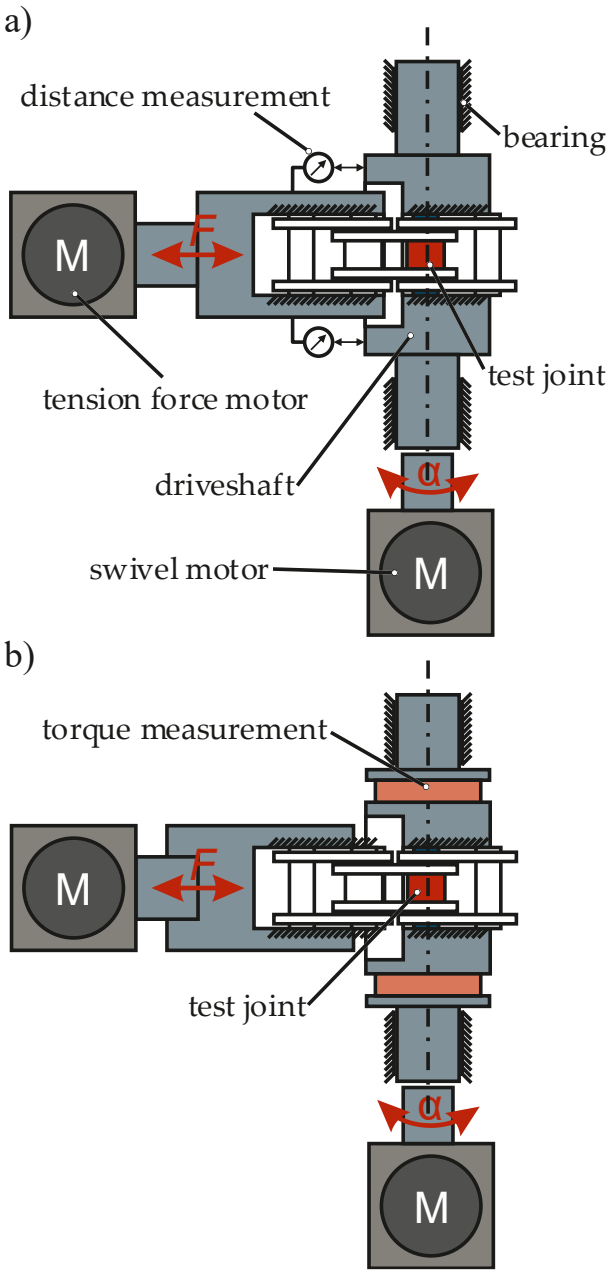

Figure 3. Schematic structure of CJT as setup for a) wear and b) friction torque measurement (Rank, et al., 2023).

2.2 Load Cycle Calculations

This study aims to demonstrate the feasibility of single-joint testing using the CJT. Therefore, the focus is not on an accurate replication of real-world loading conditions. Instead, we performed an estimation of the loading scenario based on an elite 4,000 m individual pursuit (men) track cycling race. Such bicycles typically employ a fixed gear ratio. In this analysis, a driving sprocket with $z_1 = 50$ teeth and a rear sprocket with $z_2 = 15$ teeth were assumed. The chain pitch was set to $p = 1/2"$ with a total number of $Z = 94$ chain links.

Due to the rigid and large gear ratio, the start requires a high driving torque from the cyclist. This is reflected in a very high but short power output of up to $P = 1{,}000$ W (Craig & Norton, 2001). After approximately $s = 200$ m, a constant power of $P = 550$ W is established. Since the focus of this contribution is on the implementation of the experiments, abstracted load cases are assumed. The race distance of $s = 4{,}000$ m is divided into three load segments for this purpose (Figure 4). To ensure the mechanical integrity of the test rig, deliberately high loads were selected.

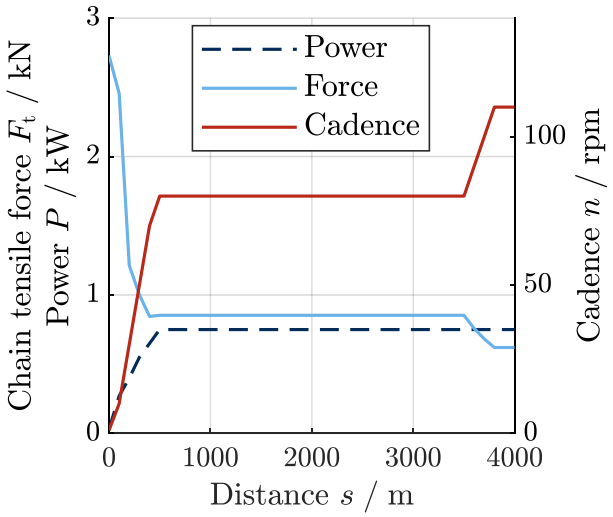

Figure 4. Estimated chain load profile during a 4,000 m individual pursuit (men) track cycling race

For improved comparability, no dynamic loads are investigated. Instead, defined steady-state loads are applied. In addition, a constant power output of $P = 750$ W is assumed. Only the ratio of torque to cadence is varied. In addition, the magnitudes are roughly estimated in the following. At the start ($s = 0 - 500$ m), the bicycle is accelerated from a standstill using high, yet decreasing torque T and chain tension force F_t, until a driving cadence of $n = 80$ rpm is reached. During the race phase ($s = 500 - 3500$ m), a constant velocity v is

maintained, while the rider produces the steady power output of approximately $P = 750\,\mathrm{W}$. Toward the end, a final sprint is assumed, during which the cadence increases to $n = 110\,\mathrm{rpm}$.

Since a suitable static cadence must be applied for the start-up phase, a chain load of $F_t = 1100\,\mathrm{N}$ is maintained. The cadence is therefore calculated as follows:

$$n = \frac{p}{2 \cdot \pi \cdot T}$$

Equation (1)

The chain speed v_{chain} is proportional to the cadence and is calculated as follows:

$$v_{\mathrm{chain}} = \pi \cdot n \cdot d$$

Equation (2)

A single load cycle N of the CJT is equivalent to one chain cycle. The time for one cycle is calculated by the chain speed and the chain length, which is determined by the number of joints X and the pitch p:

$$t_{\mathrm{rev}} = \frac{X \cdot p}{v_{\mathrm{chain}}}$$

Equation (3)

Accordingly, based on the estimation of the three load ranges, steady-state operating points are derived (Table 1). It should be noted that the chain speeds are also comparable to those in industrial applications.

Table 1. Operation Points at different load stages

Load Case	Driving cadence n/ rpm	Chain force F_t/ N	chain speed v_{chain}/ m/s	cycle time t_{rev}/ s
Start	60	1100	0.64	1.88
Mid race	80	860	0.85	1.41
Final sprint	110	620	1.16	1.02

2.3 Multi Body Simulation

To determine the loads acting within the chain joint, the chain drive is represented in a simulated environment using *Simpack*, *Dassault Systèmes* (Figure 5). The cadence C and the torque at the rear wheel T_2 serve as input parameters. The system is brought to the steady-state operating points defined in Table 1. For dynamic investigations, it must be noted that the damping and inertial properties of the system influence the chain dynamics. Validation of these properties is therefore indispensable for dynamic analyses. Furthermore, the stiffness of the contacts and components also has an effect.

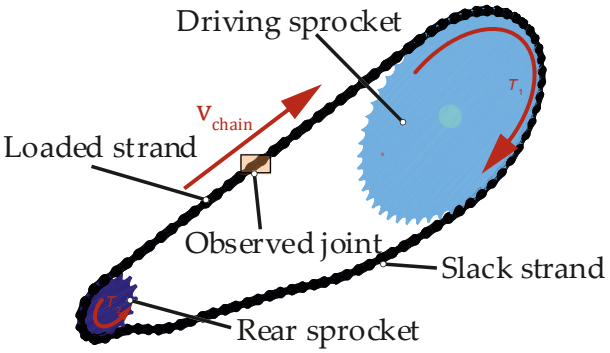

Figure 5. MBS setup with the observed joint, reproduced in CJT test, at constant chain velocity v_{chain} and loading torque T_2

Since the present study focuses on assessing the feasibility of the methodology, no validation against the actual drive is performed. In addition, only the steady-state condition is considered. Consequently, system damping and inertial effects can be neglected.

The simulation enables a steady-state analysis of an individual chain joint. The contact force and sliding velocity can be determined over a complete revolution of the chain drive. Figure 7 illustrates the contact conditions for the *Mid race* load case, beginning in the middle of the loaded strand, continuing through the engagement with the driving sprocket, the passage through the slack strand, and finally the engagement with the rear sprocket. One such revolution requires approximately $t = 1.4\,\mathrm{s}$. It must be noted that the MBS model has not been validated, and the resulting loads must therefore be interpreted as assumptions.

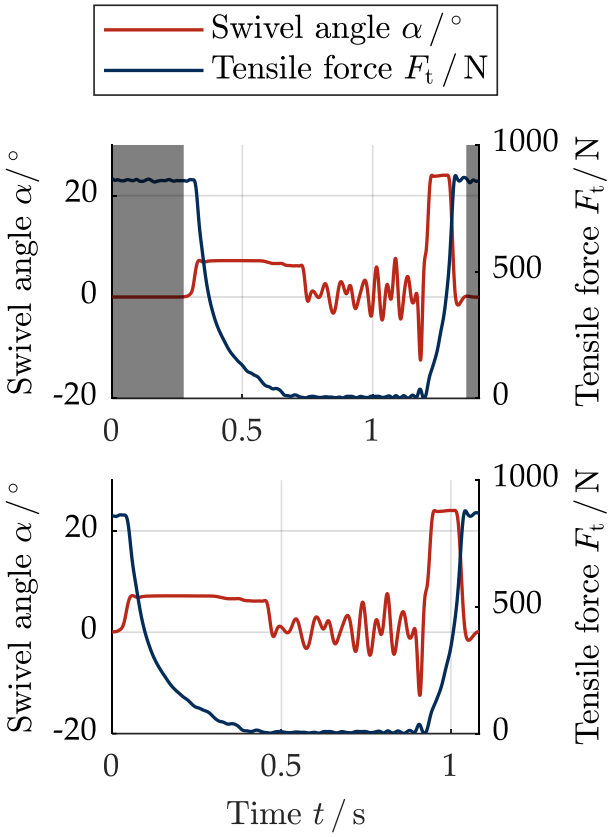

Figure 6. Representation of the individual simulated load cycle with the technically irrelevant, gray-colored areas (top) and the reduced CJT input curve derived from them (bottom)

Since only certain segments of the revolution are of mechanical interest, the cycle can be shortened, thereby significantly reducing the experimental duration. For example, in the loaded strand, a constant load is present with no sliding motion. Consequently, the segment corresponding to static loading can be omitted (Figure 6). This reduces the duration of a single revolution and thus of each individual experiment by approximately 25 %. Depending on the drive layout and vibration behavior, further reductions may be feasible, for instance in the slack strand. However, in this case, no chain tensioner is used, and significant oscillations are observed in the slack strand. Therefore, such a reduction is not applied. Oscillations in the slack strand are typical for drives without a tensioning system. These are also observed in industrial applications. Although only low normal forces occur in the slack span, the large cumulative sliding distances nevertheless affect the tribological system.

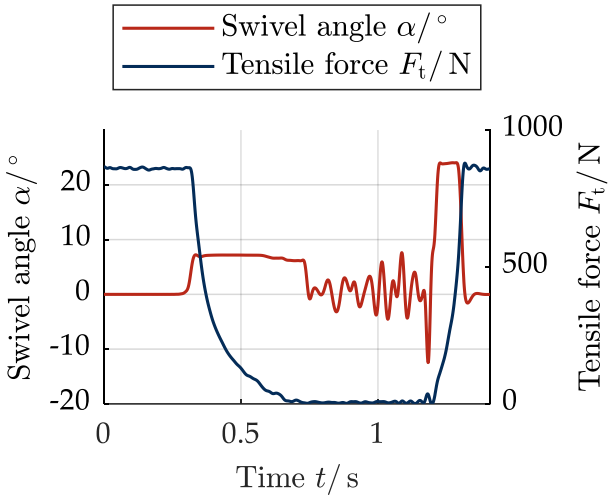

Figure 7. MBS-simulated contact conditions in the chain joint for one chain revolution in the mid-race load case

2.4 Experimental Setup

All experiments were conducted on chain links from a CN-HG701 11-speed bicycle chain by *Shimano* with a *SIL-TEC* coating. The manufacturer describes this coating as embedded fluorine particles that improve the friction and wear behavior. Since the methodological work is the primary focus, a detailed characterization of the components was omitted.

The chain is supplied with a total number of $X = 114$ links. From the complete chain, individual segments consisting of one and a half outer links and one and a half inner links were separated. For this purpose, every fifth pin was pressed out using a riveting tool. The chain segments were subsequently mounted such that the outer half-link was fixed in the linear drive adapter, while the inner half-link was fixed in the rotational shaft (Figure 8).

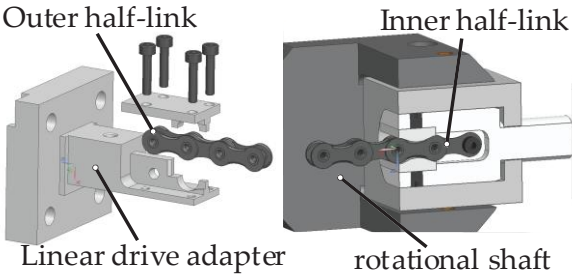

Figure 8. Assembling order of the chain segment in linear drive adapter (left) and the rotational shaft adapter (right)

The pivot shaft was then aligned so that the joint center coincided with the axis of the pivot drive. After alignment, the test run was initiated and operated continuously for $t = 24\,\text{h}$. During operation, the elongation of the chain joint was measured in real time. All experiments were carried out under initial lubrication, using only the manufacturer's transport lubricant. No cleaning or relubrication of the chain segments was performed. The tests are conducted at a controlled room temperature of $T = 21°\text{C}$ and with dehydrated air at a humidity level of up to 5 %.

2.5 Wear Analysis

Wear tests are conducted for all three load cases. Since the applicability of the methodology is the primary focus of this work, only single experiments are conducted for the three conditions for economic reasons. The experiments have a defined duration of $t = 24\,\text{h}$. To ensure uniform friction conditions, the initial lubricant applied to the chain at delivery is used. During the test execution, real-time measurement of joint elongation is performed using displacement sensors positioned between the inner and outer links. This enables a temporal evaluation of wear, allowing for the detection of anomalies and changes in wear behavior. After completion of the tests, the joints are disassembled and the bushings are cut open. The surfaces of the individual components are then examined optically using the confocal microscope µsurf Explorer, NanoFocus AG. This device enables the measurement of surface roughness and shape changes. In addition, samples in the as-new condition are characterized and compared with the worn samples.

3 Results

To contextualize the wear of the chain, it is useful to convert the test durations into comparative quantities (Table 2). For the same test duration of $t_{\text{test}} = 24\,\text{h}$ different cadences result in different numbers of load cycles N. These are calculated from the chain cycle time t_{rev} defined as the time for one complete revolution of the chain, and the test duration as follows:

$$N = \frac{t_{\text{test}}}{t_{\text{rev}}}$$

Equation (4)

The number of load cycles allows the classification of individual test runs with equal sliding distances. Auxiliary quantities that permit comparison with field tests include the chain travel distance s_{chain} and the track distance s_{track}. The chain travel distance is an equivalent to the chain length, which is the product of the number of links X and the pitch p, times the number of load cycles N:

$$s_{\text{chain}} = X \cdot p \cdot N$$

Equation (5)

The track distance is calculated by the wheel diameter, which is assumed as $d_{\text{wheel}} = 667$ mm for a 700x23c wheel, and the rear wheel speed, which is calculated by the fixed gear ratio and the cadence as described in Table 2:

$$s_{\text{track}} = \pi \cdot d_{\text{wheel}} \cdot n_1 \cdot \frac{z_1}{z_2} \cdot t_{\text{test}}$$

Equation (6)

Table 2. Test cycles for the different load stages within $t = 24\,\text{h}$

Load case	Number of load cycle N	Chain travel distance s_{chain}	Track distance s_{chain}
Start	46,000	54.9 km	603.5 km
Mid race	61,300	73.2 km	804.6 km
Final Sprint	84,300	100.7 km	1,106.4 km

The experimental data reveal differing wear behaviors for the various load spectra (Figure 9). It is again emphasized that the data are not yet statistically validated and should therefore be interpreted only as indicative trends. But all chains investigated exhibit a comparable

running-in phase within the first few load cycles. Subsequently, little to no wear is observed until a strongly progressive wear phase begins. Notably, this progressive wear occurs at similar points in time for all experiments, at approximately $N = 27{,}000$ load cycles. Up to this point, the tests display highly similar trends. Only in the final phase of the experiments do different wear rates emerge, with the *Final sprint* load spectrum in particular showing significantly lower wear.

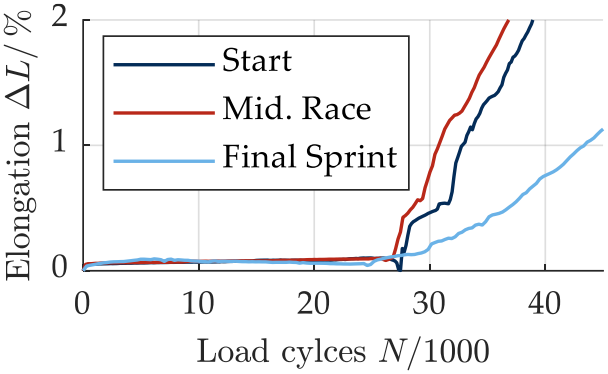

Figure 9. Link elongation ΔL vs load cycle N for the three load stages

The surface analyses also reveal pronounced signs of wear on the surfaces. Both the pins and the bushings exhibit a homogeneous and smooth surface texture when new (Figure 10). The bushings show slightly higher roughness but feature small pockets that act as lubricant reservoirs. Hardly any sharp asperities are present.

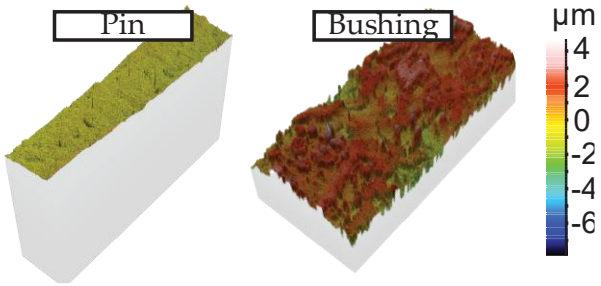

Figure 10. Representative depiction of as-new surfaces of the pin and bushing.

The surfaces of the worn samples are consistent with the characteristics observed in the wear measurements (Figure 11). The pins from the *Start* and *Mid race* load cases exhibit comparable surface morphologies, with homogeneous grooves being visible. In addition, a material ridge is observed in the center, located directly beneath the joint between the two bushing halves. Material ridges are also identifiable at the axial edges, corresponding to the air gap between the outer and inner plates.

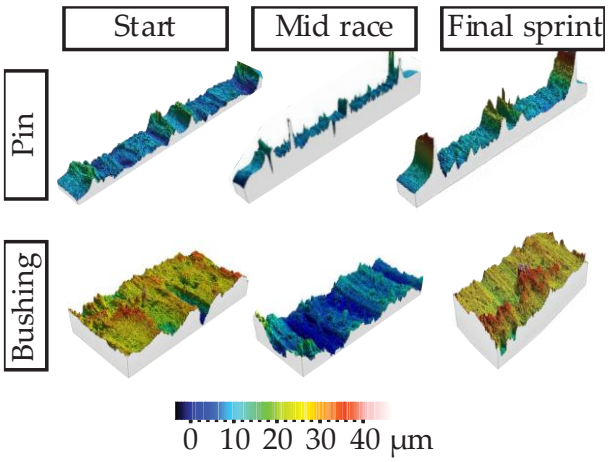

Figure 11. Depiction of worn surfaces of the pins and bushings from the different load cases.

Interestingly, the pin from the *Final sprint* load case exhibits the same characteristic shape. However, the ridges are significantly more pronounced. This is also confirmed by the roughness parameters (Table 3). While the averaged values R_a and R_z are comparable for all specimens, the absolute roughness depth R_z shows a distinct deviation.

The bushings show comparable behavior across all three load cases. Here, wear occurs over the entire surface area, producing shallow grooves. The changes are significantly smaller than those observed for the pins. This is also reflected in the fact that the roughness parameters remain nearly unchanged for all load cases. Thus, the wear of the pins appears to be the dominant mechanism. With regard to statistical significance, it must again be noted that only one test per load spectrum can be used for the evaluation.

Table 3. Roughness parameters R_a, R_z, and R_t for all specimens in the as-new condition as well as after wear induced by the respective load spectra

	Load case	R_a / µm	R_z / µm	R_t / µm
Pins	As new	0.04	0.40	1.29
	Start	0.67	4.50	25.0.
	Mid race	0.79	5.66	22.3
	Final Sprint	0.78	5.46	61.7
Bushings	As new	0.74	4.00	7.26
	Start	0.57	3.47	7.72
	Mid race	0.64	3.76	6.56
	Final Sprint	0.46	3.18	7.93

4 Discussion

The focus of this study is on demonstrating the feasibility of the testing methodology. It must therefore be noted that the wear data presented here are not statistically robust and are of only secondary relevance. The MBS simulation must first be validated to obtain reliable contact conditions. Furthermore, a more detailed lubricant analysis and a substantially larger experimental dataset will be required. Nevertheless, some initial insights can already be derived.

The wear measurements reveal a characteristic progression typical of sliding contacts, commencing with a running-in phase marked by degressive wear, followed by a linear stage and, subsequently, a progressive phase. Remarkably, the initial two phases appear nearly identical across all tests, with deviations only emerging after approximately $N = 27{,}000$ load cycles. The delayed divergence in wear behavior among the tests may be attributed to a coating failure. At the point where the wear rate increases, all three tests exhibit a similar wear magnitude of approximately 0.1 %. This may correspond to the thickness of a hardened surface layer. Once this layer has been removed, the wear rate increases significantly due to the softer underlying base material.

Another hypothesis for the wear behavior might be lubricant degradation. As wear progresses, abrasive particles from the contact partners become entrained in the lubricant. These particles adversely affect the tribological behavior. Once particle saturation increases, contact disturbances may occur, leading to the detachment of larger particles and causing a sudden increase in wear. This indicates that the lubricant film in the contact has failed. However, since no data on the lubricant is available, this hypothesis cannot be supported.

All tests were performed under identical power conditions, though with differing distributions of speed and force. The simultaneous increase in wear rate is unexpected, as the contact load and velocity have a direct influence on the lubricant film thickness. Since only one test was conducted for each load spectrum, no statistical conclusion can be drawn. Nevertheless, the trend is noteworthy. One possible explanation is the presence of a coating on the components that enhances dry-running properties and thereby reduces the influence of the lubricant. Only after $N = 27{,}000$ load cycles, the three tests exhibit different wear behaviours. This behavior is consistent with typical considerations in boundary lubrication. High forces have a negative effect, whereas higher velocities are beneficial. This supports the hypothesis that an initially favorable tribological surface layer is present, which ultimately fails as material removal progresses. To confirm this hypothesis, chemical and mechanical analyses of the surfaces in both the initial and the worn state should be carried out.

For the two load collectives *Start* and *Mid race*, the typical wear limits of $\Delta L = 2\,\%$ are already reached after $N = 40{,}000$ load cycles. Thus, a chain replacement would be required after a track distance of approximately $s_{\mathrm{track,start}} = 535\,\mathrm{km}$ for these load cases. In the

Final sprint load case, the maximum elongation of $\Delta L = 2\,\%$ is reached at $N = 56{,}000$ or $s_{\text{track}} = 735$ km.

The surface topography supports this hypothesis. In new chain joints, a high load-bearing ratio can be expected. The pins exhibit very smooth surfaces, while the bushings contain small valleys that act as lubricant reservoirs. As the surfaces undergo gradual wear, their structures evolve, and wear particles are released that may interfere with the lubricant film. The worn pin surfaces further reveal that material removal does not occur uniformly. Pronounced material ridges can be observed between the bushing halves in the pin center and at the plate interface. This appears plausible, as air gaps are present in these regions and, consequently, no contact pressure exists. The indentation of the bushing may obstruct both the ingress of fresh lubricant and the expulsion of wear particles, as the bore is partially blocked by the pin ridges. This could also be another possible explanation for the simultaneous increase in wear, which in turn may be attributable to lubricant degradation. However, to substantiate this hypothesis, chemical analyses of both the lubricant and the surfaces would be required.

The differing progressive behavior of the test setups can likewise be explained in this manner. In the *Final Sprint*, the higher sliding velocities combined with lower normal forces exert a beneficial influence on the contact. The remaining lubricant attains greater film thicknesses through hydrodynamic effects, thereby mitigating the disruptive impact of wear particles. In contrast, the other two load cases are associated with an increased asperity contact ratio, which may be further intensified by load-dependent bending of the pins.

Furthermore, wear appears to be dominated by the bushings. Although the *Final Sprint* case shows more pronounced alterations of the pins, this system exhibits the lowest overall wear.

It should be noted that the surface analysis does not allow for the determination of absolute wear. For this purpose, alternative measurement methods are mandatory. For example, the analysis of roller chains can be performed using tactile shape measurement. A wear characterization using such methods has already been established in the industrial context (Sappok & Sauer, 2015). However, adapting such methods to bicycle chains would be costly, as it requires the initial manufacturing of many new adapters, and was therefore not considered within the scope of the present study. But implementation is unlikely to pose difficulties, as the dimensions are comparable to those of industrial chains.

As lubrication was not the primary focus of this study, no detailed analysis of lubrication behavior is provided. While the same lubricant was used across all experiments to ensure consistency, no data about lubricant properties was collected, which limits the interpretation of lubrication effects on the results. Furthermore, no replication experiments were performed to provide statistical validation. Moreover, no detailed mechanical or chemical characterization of the components was performed. Future studies should respect hardness and a comprehensive analysis of the relevant material properties.

5 Practical Applications

It has been demonstrated that the Chain Joint Tribometer (CJT) enables the analysis of bicycle chain wear. All experiments were conducted without external disturbances. The methodology has proven to be promising, and further investigations can be built upon this work. In addition, initial results regarding the wear behavior of the bicycle chain were obtained. However, it should be emphasized

that the number of tests conducted was too small to allow statistically robust analyses.

In initial wear investigations, a correlation between load and wear behavior was shown. An analysis method established for industrial applications, including various auxiliary tools such as MBS and optical analysis, could be transferred to the bicycle chain system. However, these results do not yet possess statistical significance. For targeted investigations, the load spectra should be specified in greater detail, and statistical repeat tests should be performed. The MBS must also first be validated in order to represent the dynamic behavior of the chain realistically.

Surface analyses have already enabled the examination of wear-induced changes in the contact partners. In industrial contexts, such investigations are supported by shape measurements and are employed for a detailed wear analysis of the individual contact partners. Due to the substantial technical effort required, such analyses have not yet been conducted on bicycle chains. However, the findings from the experimental work suggest that these measurement methods are feasible and should be integrated into future investigations.

Furthermore, additional experimental series should be conducted to verify the hypothesis that the increase in wear after a certain number of load cycles is primarily dependent on the transmitted power. If this phenomenon can be demonstrated statistically, it would enable targeted optimization of lubricants as a function of the expected power spectrum. Combined with the implementation of efficient investigations on the CJT, this opens up significant potential both for racing applications and for the broader societal development focus of chain and lubricant manufacturers.

Another interesting field of research addresses environmental influences such as contamination, temperature or rain. Previous investigations have already focused on the influence of water ingress and contamination like dust within the chain joint. However, these effects have so far been examined only through simple tests or under field conditions. By employing the CJT, reproducible studies can be conducted under laboratory conditions. This could provide a new tool for the development of more resilient lubricants.

Funding: This research received no external funding.

Acknowledgments: The authors would like to thank the Institute for measurement and sensor technology at RPTU Kaiserslautern for their support with measurement devices and evaluation software.

Conflicts of Interest: The authors declare no conflict of interest.

References

(NAM), D. I.-N. (October 2006). *DIN ISO 10823 - Guidelines for the selection of roller chain drives.* Deutsches Institut für Normung e.V. Berlin: Beuth Verlag. DOI: 10.31030/9724581

(NATG), D. I.-N. (2018). *DIN ISO 606 - Short-pitch transmission precision roller and bush chains, attachments and associated chain and sprockets.* Tech. rep., Deutsches Institut für Normung e.V. DOI: 10.31030/2773143

Arango, I., Lopez, C., & Ceren, A. (2021). Improving the Autonomy of a Mid-Drive Motor Electric Bicycle Based on System Efficiency Maps and Its Performance. *World electric vehicle journal, 12*, 59-.

Aubert, R., Roizard, X., Grappe, F., & Lallemand, F. (2023). Tribological devices in cycling: A review. *Proceedings of the Institution of Mechanical Engineers, Part P, 0*, 17543371231202562. DOI: 10.1177/17543371231202562

Baglioni, S., Cianetti, F., & Landi, L. (2012). Influence of the addendum modification on spur gear efficiency. *Mechanism and Machine Theory, 49*, 216-233. DOI: 10.1016/j.mechmachtheory.2011.10.007

Becker, A. (2020). *Entwicklung einer Prüfmethodik für Verschleißuntersuchungen an Kettengelenken von Antriebs- und Steuerketten.* Ph.D. dissertation, Technische Universität Kaiserslautern, Technische Universität Kaiserslautern.

Becker, A., & Sauer, B. (2019). Verschleiß- und Reibungsuntersuchungen am Bolzen-Hülsen-Kontakt von Steuerketten mit einem Einzelgelenkprüfstand. *Tribologie und Schmierungstechnik, 65*, 40–47.

Becker, A., Meffert, D., & Sauer, B. (February 2019). Friction and wear investigations on single chain joints. *Forschung im Ingenieurwesen, 83*, S. 53–63. DOI: 10.1007/s10010-019-00297-x

Bobzin, K., Kalscheuer, C., Möbius, M. P., Rank, M., Oehler, M., & Koch, O. (2023). Triboactive coatings for wear and friction reduction in chain drives. *Tribology International, 185*, 108562. DOI: 10.1016/j.triboint.2023.108562

Contò, C., & Bianchi, N. (2023). E-Bike Motor Drive: A Review of Configurations and Capabilities. *Energies, 16*. DOI: 10.3390/en16010160

Craig, N. P., & Norton, K. I. (2001). Characteristics of track cycling. *Sports Med, 31*, 457–468.

Debraux, P., Manolova, A. V., Soudain-Pineau, M., & Hourde, W. (May 2013). Maximal torque and power pedaling rate relationships for high level BMX riders in field tests. *Journal of Science and Cycling, 2*, 51-57.

Fishman, E., & Cherry, C. (2016). E-bikes in the Mainstream: Reviewing a Decade of Research. *Transport Reviews, 36*, 72–91. DOI: 10.1080/01441647.2015.1069907

Galatoulas, N.-F., Genikomsakis, K. N., & Ioakimidis, C. S. (2020). Spatio-Temporal Trends of E-Bike Sharing System Deployment: A Review in Europe, North America and Asia. *Sustainability, 12*. DOI: 10.3390/su12114611

Gardner, A. S., Martin, J. C., Martin, D. T., Barras, M., & Jenkins, D. G. (01. October 2007). Maximal torque- and power-pedaling rate relationships for elite sprint cyclists in laboratory and field tests. *European Journal of Applied Physiology, 101*, 287-292. DOI: 10.1007/s00421-007-0498-4

Grau-Escolano, J., Bassolas, A., & Vicens, J. (11. July 2024). Cycling into the workshop: e-bike and m-bike mobility patterns for predictive maintenance in Barcelona's bike-sharing system. *EPJ Data Science, 13*, 48. DOI: 10.1140/epjds/s13688-024-00486-x

Kozlov, K. E., Egorov, A. V., & Belogusev, V. N. (2017). Experimental Evaluation of Chain Transmissions Lubricants Quality Using a New Method Based on Additional Inertia Moment Use. *Procedia Engineering, 206*, 617-623. DOI: 10.1016/j.proeng.2017.10.526

Li, X., Sosa, M., Andersson, M., & Olofsson, U. (2016). A study of the efficiency of spur gears made of powder metallurgy materials – ground versus super-finished surfaces. *Tribology International, 95*, 211-220. DOI: 10.1016/j.triboint.2015.11.021

Liew, Y. W., Matthews, O., Dao, D. V., & Li, H. (2025). Power Transmission Mechanism and Tribological Performance of Modern Bicycle Drivetrains—A Review. *Machines, 13*. DOI: 10.3390/machines13010066

Meffert, D., Oehler, M., & Sauer, B. (July 2021). Precise Friction Measurement in Drive Chains Using a Chain Joint Tribometer. *Tribology Online, 16*, 151–158. DOI: 10.2474/trol.16.151

Menke, W., Shaw, A., & Zhang, S. (November 2024). Cycling Power Characteristics between Instrumented and Favero Assioma Duo Road Power Meter Pedals. *Journal of Science and Cycling, 13*, 67-74. DOI: 10.28985/1324.jsc.08

Miyata, S., & Ikeda, T. (1993). *Patentnr. U.S. Patent No. 5,226,857 A.*

Nosratzadeh, H., Bhowmick, D., Carmona, A. B., Pearson, L., Thompson, J., Thai, T., & Beck, B. (2025). Implementing without evaluating: The missing link in understanding the effectiveness of financial incentive programs for e-bikes. *Cities, 156*, 105528. DOI: 10.1016/j.cities.2024.105528

Omar, M. A. (2014). Chain Drive Simulation Using Spatial Multibody Dynamics. *Advances in Mechanical Engineering, 6*, 378030. DOI: 10.1155/2014/378030

Rank, M., Meffert, D., Oehler, M., & Koch, O. (2022). Einfluss von Beschichtungen zur triboaktiven Transferschichtbildung auf die Reibung in Kettengelenken. *Tribologie und Schmierungstechnik, 69*, 5–12. DOI: 10.24053/TuS-2022-0039

Rank, M., Oehler, M., Koch, O., Bobzin, K., Kalscheuer, C., & Möbius, M. P. (2023). Investigation of the Influence of Triboactive CrAlMoN Coating on the Joint Wear of Grease-Lubricated Roller Chains. *Tribology Transactions, 66*, 1105–1116. DOI: 10.1080/10402004.2023.2264908

Sappok, D., & Sauer, B. (2015). Wear Measurement on Chain Joint Components Using a Roundness Instrument. *Periodica Polytechnica Mechanical Engineering, 59*, 51–59. DOI: 10.3311/PPme.7780

Shen, C. J., Rahim, N. A., & Rahman, M. R. (December 2022). An Investigation of Bicycle Chain Lubrication Performance in Rainy Condition. *Zulfaqar Journal of Defence Science, Engineering & Technology, 5*. Von https://zulfaqarjdset.upnm.edu.my/index.php/zjdset/article/view/94 abgerufen

Simo Kamga, L., Meffert, D., Magyar, B., Oehler, M., & Sauer, B. (2022). Simulative investigation of the influence of surface texturing on the elastohydrodynamic lubrication in chain joints. *Tribology International, 171*, 107564. DOI: 10.1016/j.triboint.2022.107564

Smit, A., van der Zwaard, S., Janssen, I., & Janssen, T. W. (14. November 2023). Power loss of the chain drive in a race tandem bicycle. *Sports Engineering, 26*, 49. DOI: 10.1007/s12283-023-00439-z

Van den Steen, N., de Geus, B., Cappelle, J., & Vanhaverbeke, L. (2022). Cycling Infrastructure for All EPACs Included? *World Electric Vehicle Journal, 13*. DOI: 10.3390/wevj13050074

Worn, R., & Dwyer, D. B. (October 2019). A novel method based on first principles to determine the accuracy and reliability of force measurements reported by bicycle power meters. *Journal of Science and Cycling, 8*, 26-31. DOI: 10.28985/jsc.v8i1.396

Zhang, S.-P., & Tak, T.-O. (2021). Efficiency Evaluation of Electric Bicycle Power Transmission Systems. *Sustainability, 13*. DOI: 10.3390/su131910988